Journal of Molecular Spectroscopy **200,** 210–228 (2000)
doi:10.1006/jmsp.1999.8037, available online at http://www.idealibrary.com on IDEAL®

Rotational Spectrum of the AsH_2 Radical in Its Ground State, Studied by Far-Infrared Laser Magnetic Resonance[1]

Rebecca A. Hughes,* John M. Brown,* and Kenneth M. Evenson†

**Physical and Theoretical Chemistry Laboratory, South Parks Road, Oxford OX1 3QZ, United Kingdom; and*
†National Institute of Standards and Technology, 325 Broadway, Boulder, Colorado 80303

Received October 4, 1999; in revised form November 22, 1999

The rotational spectrum of AsH_2 in its ground $\tilde{X}^2B_1$ electronic state has been recorded using a far-infrared laser magnetic resonance spectrometer. The AsH_2 radical was produced inside the spectrometer cavity by the reaction of arsine (AsH_3) with fluorine atoms. Hyperfine splittings from both ^{75}As and ^1H nuclei were observed, and analysis of the spectra has yielded accurate values for rotational, hyperfine, and Zeeman parameters.

INTRODUCTION

This paper describes the pure rotational spectrum of AsH_2 in its ground $\tilde{X}^2B_1$ electronic state, recorded by far-infrared (FIR) laser magnetic resonance (LMR). The analysis of the measurements has led to the determination of accurate values for the rotational, hyperfine, and Zeeman parameters.

The first observation of AsH_2 was by Dixon and co-workers (*1, 2*), who detected absorption bands in the $\tilde{A}^2A_1$–$\tilde{X}^2B_1$ electronic transition of AsH_2 and AsD_2 and determined fairly accurate values for rotational, centrifugal distortion, and spin–rotation parameters of AsH_2 in its ground state. Basco and Yee (*3*) observed the same electronic transition in absorption at lower resolution, while Ni *et al.* (*4*) investigated it in emission and obtained an approximate value for the bending vibrational frequency ν_2. The EPR spectrum has been observed in a matrix (*5*), but, because the hyperfine splittings were unresolved, no hyperfine parameters were determined. The rotation–vibration spectra due to the bending (*6*) and one or both of the stretching modes have been observed by mid-IR LMR, the latter during a study of AsH by the present authors (*7*), but both spectra have so far proved too difficult to analyze given the existing knowledge of the radical. Concurrent with the present work, Saito and co-workers observed the rotational spectra of AsH_2 and AsD_2 using rotational spectroscopy at millimeter wavelengths (*8, 9*). Theoretical studies have provided estimates of the geometry and harmonic vibrational frequencies (*10*) and bond dissociation energies (*11, 12*) of AsH_2.

The objective of this study was to refine the ground state parameters of AsH_2, both for its own sake and also to help with the analysis of the mid-IR spectra. Although the motivation for studying AsH_2 was primarily academic, namely to follow the trends down Group V from the much-studied NH_2 and PH_2 to the less well-characterized AsH_2, it is worth noting that AsH_2 is involved as a reaction intermediate in the production of GaAs semiconductors by chemical vapor deposition. GaAs is of great interest since it has many practical applications. It is used in detectors (for example, in radiology), diodes, electrodes, transistors, and solar cells; over 2000 papers relating to GaAs were published in 1998 alone. Despite its widespread use, the thermodynamics and kinetics of the many reactions involved in the production of GaAs are not yet completely understood.

EXPERIMENTAL DETAILS

The FIR LMR spectrometer at NIST, Boulder, CO, was used in this study and has been described in detail elsewhere (*13*). The FIR radiation was generated in a chosen laser gas which is optically pumped by the appropriate line of an infrared CO_2 laser. Part of the FIR radiation was coupled out of the laser cavity and detected with a liquid-helium-cooled In:Sb detector. The resonance signals were modulated at 39 kHz using Zeeman modulation coils and amplified by a lock-in amplifier tuned to this frequency.

The radical AsH_2 was formed in the intracavity cell of the spectrometer by the reaction of fluorine atoms with arsine, AsH_3. The fluorine atoms were generated by passing a 10% mixture of molecular fluorine in helium through a microwave discharge. The optimum gas conditions were 30 mTorr (4 Pa) AsH_3 and 100 mTorr (13.3 Pa) F_2/He, with around 810 mTorr (108 Pa) of helium as a flow gas.

Laser lines were selected for searching on the basis of predictions made using the best available parameters (*2*). The external magnetic field was scanned and spectra in both per-

[1] Supported in part by NASA Contract W-18,623.

0022-2852/00 $35.00

pendicular ($\Delta M_J = \pm 1$) and parallel ($\Delta M_J = 0$) polarizations were recorded. A large number of spectra were recorded; due to time constraints, some of these were measured on somewhat broader scans than usual. The accuracy of the measurements is $\sim \pm 0.01$ mT for $B \leq 0.1$ T and $\pm 1 \times 10^{-4}$ B for $B > 0.1$ T.

OBSERVATIONS AND ANALYSIS

Background

AsH_2 is a bent molecule and so has the inertial properties of an asymmetric top. As a result of this, the double degeneracy of the $|K|$ levels (where $|K|$ is the projection of the rotational angular momentum N along the near-symmetric top axis) is removed and the levels are labeled $N_{K_aK_c}$, where K_a and K_c are the values of $|K|$ with which the level correlates in the prolate and oblate symmetric top limits, respectively. The asymmetry doubling is first order for $K_c{}^2 = 1$ only, higher order effects splitting levels with $K_c > 1$. Therefore the asymmetry splitting decreases with increasing K_c and at high values of K_c is negligible.

Each rotational level N is split by the spin–rotation interaction $\mathbf{J} = \mathbf{N} + \mathbf{S}$. For AsH_2 which has an electron spin angular momentum S of $\frac{1}{2}$ there are two spin–rotation components for each rotational level, $J = N + \frac{1}{2}$ (F_1) and $J = N - \frac{1}{2}$ (F_2), where F_i labels the spin–rotation components in increasing energy order for a given J value. Figure 1 shows the energy levels of AsH_2 in its ground electronic state (free of hyperfine and Zeeman effects) arranged with K_c along the horizontal axis. For $K_c > 1$, the spin–rotation splitting is greater than the asymmetry doubling.

Interactions which involve the nuclear spins of the arsenic nucleus ($I_{^{75}As} = \frac{3}{2}$)[3] and the two equivalent hydrogen nuclei ($I_{^1H} = \frac{1}{2}$) cause hyperfine splittings. The arsenic nucleus gives rise to a quartet splitting. The hydrogen nuclei can contribute to the hyperfine pattern in two ways: the three symmetric combinations ($I_{total} = 1$; *ortho*) give rise to a triplet splitting of each member of the quartet, while the one antisymmetric combination ($I_{total} = 0$; *para*) produces no further splitting. Due to the symmetry requirement of the total wavefunction with respect to permutation of the hydrogen nuclei, the *ortho* combinations occur when the rotational wavefunction is symmetric (K_c, K_a both odd or both even) and the *para* combination when it is antisymmetric (K_c, K_a odd, even or even, odd). Note that the two component levels of an asymmetry doublet for a near-oblate top have the same parity but opposite *ortho*/*para* character. The permanent electric dipole moment of AsH_2 lies along the b inertial axis; consequently rotational transitions obey b-type selection rules.

[2] AsH_2 is a near-oblate rotor ($\kappa = 0.805$) so the asymmetry splitting can be regarded as a doubling of the K_c levels into two levels with the same value of K_c but different values of K_a.

[3] ^{75}As is the only isotope of arsenic.

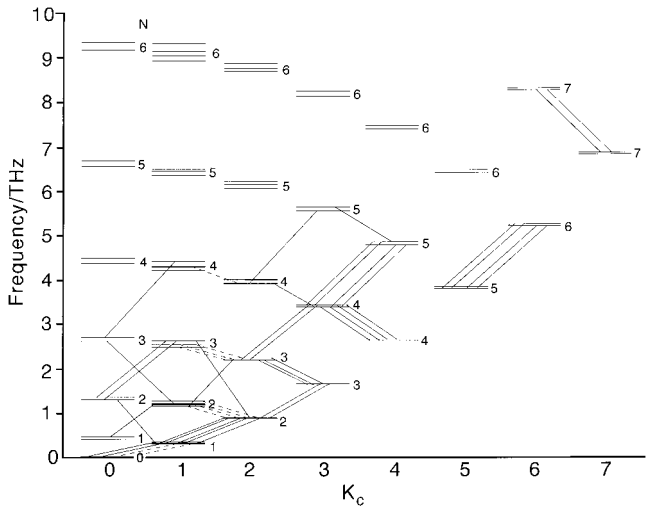

FIG. 1. Spin–rotational energy levels (free of hyperfine and Zeeman effects) of AsH_2 in its ground state calculated from the determined parameters, arranged with K_c along the horizontal axis. For $K_c > 1$, the spin–rotation splitting is greater than the asymmetry splitting. For each rotational level N, the F_1 spin component lies *below* the F_2 component. The observed FIR transitions (solid lines) and the millimeter-wave transitions (*8*) (dotted lines) are also shown.

The interaction of the molecule with the external magnetic field gives rise to a Zeeman splitting of the levels. Each level J is split into $2J + 1$ M_J components where M_J is the projection of J along the external field direction. Transitions obey the selection rules $\Delta M_J = 0, \pm 1$ according to the polarization of the oscillating electric field with respect to the external magnetic field.

Observations and Assignment

FIR LMR spectra attributed to AsH_2 in its ground $\tilde{X}^2B_1$ electronic state have been observed on 14 different laser lines. Details of the laser lines and the rotational transitions observed on them are given in Table 1. The energy level diagram of Fig. 1 is a summary of these observations[4] (solid lines) together with the observations made in the millimeter-wave study (*8*) (dotted lines). Table 2 gives the detailed measurements and assignments of the resonances. The assignment of the spectra was based on the best available parameters in the literature guided by predictions of the Zeeman patterns.

Examples of the spectra are given in Figs. 2, 3, and 4. Figure 2 shows part of the 232.9-μm (1.287 THz) spectrum recorded in parallel polarization. The quartet of triplets marked *a* is due to AsH_2 (*ortho*) in its ground state. The quartets of doublets *b*, *c* correspond to AsH in its ground $^3\Sigma^-$ and first excited $^1\Delta$

[4] Transitions due to individual Zeeman and hyperfine components are not indicated.

TABLE 1

Observed Transitions in the Rotational Spectrum of AsH_2, with the Details of the FIR Laser Lines Used to Record Them

laser line/GHz	laser line/μm	laser gas	CO_2 pump line	AsH_2 transition	
				$N_{K_aK_c}$	F_i^a
337.1919	889.078	CH_2CF_2	10P22′	$1_{11} - 0_{00}$	$F_1 - F_1$
337.2770	888.854	CH_2CF_2	10P22″	$1_{11} - 0_{00}$	$F_1 - F_1$
					$F_2 - F_2$
538.3473	556.871	CD_3I	10P36	$2_{02} - 1_{11}$	$F_1 - F_1$
				$2_{12} - 1_{01}$	$F_1 - F_1$
554.1590	540.986	CH_2F_2	9R42	$2_{02} - 1_{11}$	$F_2 - F_1$
				$2_{12} - 1_{01}$	$F_2 - F_1$
					$F_2 - F_2$
				$3_{12} - 3_{03}$	$F_1 - F_1$
					$F_2 - F_2$
				$3_{22} - 3_{13}$	$F_1 - F_1$
				$4_{32} - 4_{23}$	$F_1 - F_1$
783.4860	382.636	CH_2F_2	9R10″	$2_{21} - 1_{10}$	$F_1 - F_1$
				$3_{03} - 2_{12}$	$F_2 - F_1$
				$3_{13} - 2_{02}$	$F_2 - F_1$
				$4_{13} - 4_{04}$	$F_2 - F_2$
					$F_1 - F_1$
				$4_{23} - 4_{14}$	$F_2 - F_2$
					$F_1 - F_1$
				$5_{33} - 5_{24}$	$F_2 - F_2$
973.2243	308.038	CH_2DOH	9P14	$2_{20} - 1_{11}$	$F_1 - F_1$
				$3_{22} - 2_{11}$	$F_1 - F_1$
1256.8720	238.523	$^{13}CH_3OH$	9P12′	$3_{31} - 2_{20}$	$F_2 - F_2$
				$4_{13} - 3_{22}$	$F_2 - F_1$
1262.1617	237.521	$^{13}CH_3OH$	9P12″	$3_{31} - 2_{20}$	$F_2 - F_2$
				$4_{23} - 3_{12}$	$F_2 - F_1$
1286.9995	232.937	CH_3OH	9R10	$3_{31} - 2_{20}$	$F_2 - F_1$
1302.8458	230.106	CH_2F_2	9R42	$3_{31} - 2_{20}$	$F_2 - F_1$
1397.1186	214.577	CH_2F_2	9R34	$3_{30} - 2_{21}$	$F_1 - F_1$
				$6_{06} - 5_{15}$	$F_1 - F_1$
				$6_{16} - 5_{05}$	$F_1 - F_1$
				$7_{16} - 7_{07}$	$F_1 - F_2$
				$7_{26} - 7_{17}$	$F_1 - F_2$
1419.0493	211.261	CH_3OH	10R4	$5_{14} - 4_{23}$	$F_1 - F_1$
					$F_2 - F_2$
				$5_{24} - 4_{13}$	$F_1 - F_1$
					$F_2 - F_2$
				$6_{06} - 5_{15}$	$F_2 - F_1$
				$6_{16} - 5_{05}$	$F_2 - F_1$
1626.6026	184.306	CH_2F_2	9R32	$5_{23} - 4_{32}$	$F_1 - F_1$
1726.5485	173.637	$^{13}CD_3OD$	10R20	$3_{31} - 2_{02}$	$F_2 - F_2$
				$4_{41} - 3_{30}$	$F_2 - F_2$

Note. F_i labels the spin-rotation components in order of increasing energy for a given value of J.

states, respectively. The broad signals marked *d* are due to NH_2 in its ground state; NH_2 is probably formed from the small amount of N_2 present as an impurity in the fluorine. The production of AsH_2 was optimized over that of AsH by increasing the proportion of arsine in the gas mixture. Figure 3, recorded using the 382.6-μm (0.783 THz) laser line in parallel polarization, shows the spectrum arising from two Zeeman components of the asymmetry doublet 3_{13}–2_{02} (F_2–F_1), 3_{03}–2_{12} (F_2–F_1). The quartets of triplets (*ortho*) correspond to the former transition and the quartets of singlets (*para*) to the latter. The stronger signals have $M_J = -\frac{5}{2}$–$(-\frac{5}{2})$, while the weaker signals have $M_J = -\frac{3}{2}$–$(-\frac{3}{2})$. Figure 4 is part of the spectrum recorded using the 211.3-μm (1.419 THz) laser line in parallel polarization. These signals are the result of one Zeeman component ($M_J = \frac{11}{2}$–$\frac{11}{2}$) of the asymmetry doublet 6_{06}–5_{15} (F_2–F_1), 6_{16}–5_{05} (F_2–F_1). The quartet of triplets and quartet of singlets arising from these transitions are completely overlapped to give a 1:2:1 intensity pattern, a mani-

TABLE 2

Details of the Observed Resonances and the Least-Squares Fit for AsH_2 in the $v = 0$ Level of the $\tilde{X}^2B_1$ Ground State

$N_{K_aK_c}$	J	M_J	$M_{I_{As}}$	M_{I_H}	field mT	tuning rate MHz/mT	obs - calc MHz
			laser frequency = 337.1919 GHz				
$1_{11} - 0_{00}$	3/2 − 1/2	1/2 − -1/2	3/2	-1	941.4	5.4	-0.4
				0	943.2	5.4	-0.6
				1	944.9	5.4	-0.3
			1/2	-1	946.6	5.4	0.6
				0	948.5	5.4	-0.2
				1	950.3	5.4	-0.4[b]
			-1/2	-1	950.9	5.4	0.3[b]
				0	952.6	5.4	0.6
				1	954.0	5.4	2.6[b]
			-3/2	-1	954.5	5.4	-2.7[b]
				0	955.7	5.4	0.4
				1	957.5	5.4	0.2
			laser frequency = 337.2770 GHz				
$1_{11} - 0_{00}$	3/2 − 1/2	1/2 − -1/2	3/2	0	959.3	5.3	-1.3
			1/2	0	964.7	5.2	-1.1
			-1/2	0	968.8	5.3	-0.4
			-3/2	0	971.7	5.3	0.0
	2 − 1[a]	1/2 − 1/2	3/2	-1	1839.9	-1.7	-0.1
				0	1841.3	-1.7	0.2
				1	1842.5	-1.7	0.1
			1/2	-1	1913.4	-1.6	0.6
				0	1914.7	-1.6	0.8
				1	1915.9	-1.6	0.8
			-1/2	-1	1975.4	-1.5	1.5
				0	1976.6	-1.5	1.6
				1	1977.7	-1.5	1.5
			-3/2	-1	2022.8	-1.4	2.7[b]
				0	2024.2	-1.4	3.0[b]
				1	2025.2	-1.4	2.8[b]
			laser frequency = 538.1590 GHz				
$2_{02} - 1_{11}$	5/2 − 3/2	3/2 − 3/2	-3/2	-1	207.9	-10.0	1.2[b]
				0	209.6	-10.0	0.6[b]
				1	210.6	-10.0	-7.1[b]
			-1/2	-1	211.4	-10.1	8.4[b]
				0	211.4	-10.1	-9.3[b]
				1	211.8	-10.0	-23.0[b]
			1/2	-1	212.4	-10.1	7.1[b]
				0	213.1	-10.1	-3.6[b]
				1	213.5	-10.0	-17.4[b]
			3/2	-1	214.1	-10.1	28.1[b]
				0	214.9	-10.1	18.4[b]
				1	215.3	-10.0	4.6[b]
		1/2 − 1/2	-3/2	-1	457.6	-4.3	1.3
				0	459.4	-4.3	1.3
				1	461.1	-4.3	0.9
			-1/2	-1	465.2	-4.3	0.9
				0	467.0	-4.3	1.0
				1	468.8	-4.3	1.0
			1/2	-1	471.4	-4.2	1.1
				0	473.1	-4.2	0.7
				1	474.9	-4.2	0.7[b]
			3/2	-1	475.9	-4.2	0.6[b]
				0	477.7	-4.2	0.7
				1	479.5	-4.2	0.7
$2_{12} - 1_{01}$	5/2 − 3/2	3/2 − 3/2	3/2	0	660.3	-20.6	0.7
			1/2	0	661.2	-20.5	2.4
			-1/2	0	662.6	-20.4	2.0
			-3/2	0	664.6	-20.2	1.1

[a] Where J is not a good quantum number, the value of F_i (1 or 2) is used instead. F_i labels the spin-rotation components in order of increasing energy for a given value of J.

[b] This point given zero weight in the fit.

TABLE 2—*Continued*

$N_{K_a K_c}$	J	M_J	$M_{I_{As}}$	M_{I_H}	flux density mT	tuning rate MHz/mT	obs - calc MHz
			laser frequency = 554.1590 GHz				
$2_{02} - 1_{11}$	3/2 − 3/2	3/2 − 3/2	3/2	-1	126.0	-20.3	1.5
				0	127.7	-20.3	0.9
				1	129.5	-20.3	1.9
			1/2	-1	137.1	-19.7	2.7
				0	138.8	-19.7	2.1
				1	140.6	-19.7	3.0
			-1/2	-1	149.0	-19.3	1.0
				0	150.7	-19.3	0.4
				1	152.5	-19.3	1.3
			-3/2	-1	162.2	-19.0	-0.1
				0	164.0	-19.0	1.2
				1	165.6	-19.0	-1.6
$2_{12} - 1_{01}$	2 − 1[a]	3/2 − 3/2	3/2	0	798.4	-5.4	1.2
			1/2	0	835.1	-5.0	0.7
			-1/2	0	873.2	-4.7	0.1
			-3/2	0	912.8	-4.4	-0.3
	2 − 2[a]	1/2 − 1/2	3/2	0	816.0	-3.0	0.1
			1/2	0	832.2	-2.9	0.2
			-1/2	0	842.6	-2.8	0.0
			-3/2	0	846.3	-2.7	0.2
	3/2 − 1/2	1/2 − -1/2	3/2	0	292.3	-7.9	1.0
			1/2	0	312.7	-7.7	1.6
			-1/2	0	334.0	-7.4	0.9
			-3/2	0	356.1	-7.2	0.5
		3/2 − 1/2	3/2	0	314.3	-10.7	-0.1
			1/2	0	324.9	-10.6	0.0
			-1/2	0	335.8	-10.5	-0.6
			-3/2	0	347.3	-10.4	0.2
$3_{12} - 3_{03}$	1 − 1[a]	3/2 − 3/2	-3/2	0	1834.6	4.9	2.4
			-1/2	0	1840.5	4.9	2.2
			1/2	0	1846.9	4.9	2.6
			3/2	0	1853.8	4.9	2.7
	7/2 − 7/2	1/2 − -1/2	-3/2	0	1962.6	3.5	-1.1
			-1/2	0	1991.7	3.4	-2.4
			1/2	0	2015.2	3.3	-3.5
			3/2	0	2033.0	3.3	-4.2
	2 − 2[a]	5/2 − 3/2	-3/2	0	1606.6	-8.5	1.9
			-1/2	0	1618.7	-8.4	2.5
			1/2	0	1632.3	-8.3	3.1
			3/2	0	1647.4	-8.2	2.1
$3_{22} - 3_{13}$	1 − 1[a]	5/2 − 5/2	3/2	-1	994.2	14.1	-0.3[b]
				0	995.0	14.1	13.5[b]
				1	995.9	14.1	26.0[b]
			1/2	-1	996.8	14.0	-24.2[b]
				0	997.3	14.0	-6.3[b]
				1	997.7	14.0	13.0[b]
			-1/2	-1	998.6	13.8	-17.7[b]
				0	999.1	13.8	0.0[b]
				1	1000.9	13.8	-0.2[b]
			-3/2	-1	1000.9	13.7	0.4[b]
				0	1002.6	13.7	1.5[b]
				1	1004.4	13.7	1.3[b]
	7/2 − 7/2	1/2 − -1/2	-3/2	-1	1089.3	6.8	-0.9
				0	1091.1	6.8	-0.7
				1	1092.9	6.8	-0.4
			-1/2	-1	1100.1	6.7	-0.7
				0	1101.9	6.7	-0.4
				1	1103.7	6.7	-0.1
			1/2	-1	1108.1	6.6	-0.4
				0	1109.9	6.6	-0.1
				1	1111.7	6.6	0.1
			3/2	-1	1113.5	6.6	-0.4
				0	1115.2	6.6	0.5
				1	1117.0	6.6	0.8

TABLE 2—*Continued*

$N_{K_aK_c}$	J	M_J	$M_{I_{As}}$	M_{I_H}	flux density mT	tuning rate MHz/mT	obs - calc MHz
	7/2 − 7/2	-1/2 − -3/2	-3/2	-1	1533.2	3.7	-1.6
				0	1535.0	3.7	-1.4
				1	1536.9	3.7	-1.6
			-1/2	-1	1544.4	3.6	-1.4
				0	1546.2	3.6	-1.2
				1	1548.0	3.6	-1.1
			1/2	-1	1551.6	3.6	-0.8
				0	1553.5	3.6	-1.0
				1	1555.4	3.6	-1.2[b]
			3/2	-1	1555.4	3.5	-0.6[b]
				0	1557.4	3.5	-1.2
				1	1559.2	3.5	-1.0
	1 − 1[a]	3/2 − 5/2	3/2	-1	1602.9	7.0	0.3
				0	1604.7	7.0	-0.1
				1	1606.6	7.0	-1.2
			1/2	-1	1610.7	6.9	-0.1
				0	1612.4	6.9	0.2
				1	1614.1	6.9	0.5
			-1/2	-1	1621.6	6.8	0.3
				0	1623.4	6.8	-0.1
				1	1625.1	6.8	0.2
			-3/2	-1	1635.7	6.7	0.5
				0	1637.4	6.7	0.8
				1	1639.1	6.7	1.1
$4_{32} - 4_{23}$	1 − 1[a]	3/2 − 3/2	-3/2	0	1584.9	3.4	-8.5[b]
			-1/2	0	1599.0	3.4	-8.2[b]
			1/2	0	1611.6	3.4	-8.3[b]
			3/2	0	1622.7	3.4	-8.7[b]
			laser frequency = 783.4860 GHz				
$2_{21} - 1_{10}$	5/2 − 3/2	-1/2 − -3/2	-3/2	0	1137.1	5.8	1.9
			-1/2	0	1147.9	5.8	1.8
			1/2	0	1157.8	5.7	2.7
			3/2	0	1167.0	5.7	2.7
		1/2 − -1/2	3/2	0	1205.3	6.7	0.6
			1/2	0	1206.8	6.7	0.0
			-1/2	0	1211.4	6.6	0.1
			-3/2	0	1219.0	6.6	1.4
		3/2 − 1/2	3/2	0	1285.7	8.8	-0.6
			1/2	0	1287.8	8.8	-0.2
			-1/2	0	1289.3	8.8	-0.2
			-3/2	0	1290.2	8.8	-0.4
$3_{03} - 2_{12}$	5/2 − 5/2	-5/2 − -5/2	3/2	0	127.5	24.9	-3.1
			1/2	0	140.5	25.0	-3.3
			-1/2	0	154.8	25.2	-1.5
			-3/2	0	170.3	25.6	-2.3
		-3/2 − -3/2	3/2	0	197.1	18.9	-1.5
			1/2	0	207.9	19.3	-1.0
			-1/2	0	219.1	19.8	1.3
			-3/2	0	230.7	20.4	0.8
$3_{13} - 2_{02}$	5/2 − 5/2	-5/2 − -5/2	3/2	-1	93.4	24.5	-4.8
				0	95.1	24.5	-4.8
				1	96.8	24.5	-4.0
			1/2	-1	106.5	24.6	-4.6
				0	108.1	24.6	-2.1
				1	109.9	24.6	-3.7
			-1/2	-1	121.1	24.9	-0.7
				0	122.9	24.9	-3.1
				1	124.6	24.9	-2.3
			-3/2	-1	137.1	25.4	-0.6
				0	138.8	25.4	-0.5
				1	140.5	25.4	0.3
		-3/2 − -3/2	3/2	-1	151.3	18.0	-0.7
				0	153.0	18.0	-0.5
				1	154.8	18.0	-1.8
			1/2	-1	163.0	18.4	-1.9

TABLE 2—*Continued*

$N_{K_aK_c}$	J	M_J	$M_{I_{As}}$	M_{I_H}	flux density mT	tuning rate MHz/mT	obs - calc MHz
				0	164.6	18.4	0.1
				1	166.3	18.4	0.7
			-1/2	-1	175.3	19.0	0.2
				0	177.0	19.0	0.5
				1	178.7	19.0	1.1
			-3/2	-1	188.1	19.8	1.2
				0	189.8	19.8	1.5
				1	191.6	19.8	0.2
		1/2 – -1/2	-3/2	-1	356.3	14.5	0.8
				0	358.1	14.5	0.7
				1	359.8	14.5	2.3[b]
			-1/2	-1	359.8	14.4	-0.3[b]
				0	361.5	14.4	1.1
				1	363.3	14.4	1.1[b]
			1/2	-1	363.3	14.3	2.0[b]
				0	365.1	14.3	1.9
				1	366.9	14.3	2.0[b]
			3/2	-1	366.9	14.2	2.6[b]
				0	368.7	14.2	2.6
				1	370.6	14.2	1.2
$4_{13} - 4_{04}$	1 – 1[a]	7/2 – 7/2	3/2	-1	1709.9	10.6	-1.2[b]
				0	1711.5	10.6	0.1[b]
				1	1713.3	10.6	-0.6[b]
			1/2	-1	1720.5	10.4	-1.5
				0	1722.1	10.4	-0.2
				1	1723.9	10.4	-0.9
			-1/2	-1	1733.2	10.3	-0.2
				0	1734.9	10.3	0.1
				1	1736.6	10.3	0.4
			-3/2	-1	1748.0	10.2	1.7
				0	1749.8	10.2	0.9
				1	1751.6	10.2	0.2
	2 – 2[a]	7/2 – 7/2	3/2	-1	1628.7	-11.4	2.1[b]
				0	1630.4	-11.4	1.2[b]
				1	1632.2	-11.4	1.3[b]
			1/2	-1	1632.5	-11.4	0.6[b]
				0	1634.4	-11.4	2.0[b]
				1	1636.1	-11.4	1.0[b]
			-1/2	-1	1636.1	-11.3	2.9[b]
				0	1637.8	-11.3	1.9[b]
				1	1638.8	-11.3	-7.0[b]
			-3/2	-1	1638.5	-11.3	-2.4[b]
				0	1640.6	-11.3	1.1[b]
				1	1642.4	-11.3	1.3[b]
$4_{23} - 4_{14}$	1 – 1[a]	7/2 – 7/2	3/2	0	1661.4	11.2	-3.1
			1/2	0	1671.3	11.1	-2.6
			-1/2	0	1683.3	11.0	-2.3
			-3/2	0	1697.2	10.8	-0.8
		5/2 – 3/2	-3/2	0	1866.3	6.9	-0.3
			-1/2	0	1872.9	6.9	-0.6
			1/2	0	1878.7	6.8	0.6
			3/2	0	1883.9	6.8	0.3
	2 – 2[a]	7/2 – 7/2	3/2	0	1704.6	-10.9	0.6
			1/2	0	1708.9	-10.8	0.4[b]
			-1/2	0	1712.7	-10.8	0.5[b]
			-3/2	0	1715.9	-10.8	-0.1
$5_{33} - 5_{24}$	9/2 – 9/2	9/2 – 7/2	-3/2	-1	1729.6	-9.4	-1.4
				0	1731.4	-9.4	-1.8
				1	1733.3	-9.4	-1.3
			-1/2	-1	1738.7	-9.4	-0.4
				0	1740.5	-9.4	-0.8
				1	1742.4	-9.4	-0.3
			1/2	-1	1747.1	-9.5	-1.0
				0	1748.9	-9.5	-1.4
				1	1750.8	-9.5	-0.8
			3/2	-1	1755.0	-9.5	-1.4
				0	1756.9	-9.5	-0.8
				1	1758.7	-9.5	-1.2

TABLE 2—*Continued*

$N_{K_aK_c}$	J	M_J	$M_{I_{As}}$	M_{I_H}	flux density mT	tuning rate MHz/mT	obs - calc MHz
			laser frequency = 973.2243 GHz				
$2_{20} - 1_{11}$	5/2 − 3/2	3/2 − 3/2	3/2	-1	126.8	-6.3	0.9
				0	128.4	-6.3	0.7
				1	130.1	-6.3	0.9
			1/2	-1	144.1	-6.4	2.0
				0	145.6	-6.3	1.1
				1	147.3	-6.3	1.3
			-1/2	-1	159.1	-6.4	0.8
				0	160.8	-6.4	1.1
				1	162.5	-6.4	1.3
			-3/2	-1	172.2	-6.4	0.4
				0	173.9	-6.4	0.7
				1	175.6	-6.4	0.9
$3_{22} - 2_{11}$	7/2 − 5/2	5/2 − 5/2	-3/2	-1	1922.6	-20.0	-14.0[b]
				0	1922.6	-20.0	-50.1[b]
				1	1923.2	-20.0	-74.3[b]
			-1/2	-1	1923.9	-20.0	27.1[b]
				0	1924.4	-20.0	1.0[b]
				1	1924.4	-20.0	-35.2[b]
			1/2	-1	1925.1	-20.1	46.9[b]
				0	1925.6	-20.0	20.7[b]
				1	1926.2	-20.0	-3.5[b]
			3/2	-1	1926.2	-20.1	45.9[b]
				0	1926.9	-20.1	23.7[b]
				1	1927.5	-20.1	-0.5[b]
			laser frequency = 1256.8720 GHz				
$3_{31} - 2_{20}$	5/2 − 3/2	-3/2 − -3/2	-3/2	-1	1574.8	-2.2	6.0[b]
				0	1576.8	-2.2	5.9[b]
				1	1578.8	-2.2	5.7[b]
			-1/2	-1	1608.7	-2.2	5.9[b]
				0	1610.7	-2.2	5.8[b]
				1	1612.7	-2.2	5.6[b]
			1/2	-1	1649.2	-2.2	5.9[b]
				0	1651.2	-2.2	5.8[b]
				1	1653.4	-2.2	6.0[b]
			3/2	-1	1696.6	-2.1	5.2[b]
				0	1698.7	-2.1	5.2[b]
				1	1700.7	-2.1	5.1[b]
$4_{13} - 3_{22}$	7/2 − 7/2	-7/2 − -7/2	3/2	-1	208.2	25.8	0.4
				0	210.0	25.8	-0.6
				1	211.8	25.8	-1.2
			1/2	-1	212.3	25.8	-0.8
				0	214.0	25.8	0.8
				1	215.8	25.8	0.2
			-1/2	-1	216.2	25.8	0.9
				0	218.0	25.8	-0.1
				1	219.8	25.8	-0.7
			-3/2	-1	220.1	25.8	-0.4
				0	221.8	25.8	1.2
				1	223.6	25.8	0.6
		-5/2 − -5/2	3/2	-1	279.9	20.2	1.0
				0	281.7	20.2	0.1
				1	283.4	20.2	1.4[b]
			1/2	-1	283.7	20.2	0.8[b]
				0	285.4	20.2	1.9
				1	287.2	20.2	1.2[b]
			-1/2	-1	287.5	20.2	0.6[b]
				0	289.2	20.2	1.7
				1	291.0	20.2	1.0[b]
			-3/2	-1	291.3	20.3	0.2[b]
				0	293.0	20.3	1.3
				1	294.7	20.3	2.7

TABLE 2—*Continued*

$N_{K_aK_c}$	J	M_J	$M_{I_{As}}$	M_{I_H}	flux density mT	tuning rate MHz/mT	obs - calc MHz
			laser frequency = 1262.9995 GHz				
$3_{31} - 2_{20}$	5/2 − 3/2	3/2 − 3/2	-3/2	-1	477.8	1.7	-0.1
				0	479.8	1.7	0.3
				1	481.8	1.7	0.7
			-1/2	-1	545.8	1.5	-0.4
				0	547.8	1.5	0.0
				1	550.8	1.5	-1.1
			1/2	-1	619.8	1.3	-0.2
				0	621.8	1.3	0.3
				1	623.8	1.3	0.7
			3/2	-1	703.7	1.1	-0.4
				0	705.7	1.1	0.1
				1	708.7	1.1	-0.4
		1/2 − 3/2	-3/2	-1	146.1	6.5	-1.3
				0	147.9	6.5	-0.9
				1	149.8	6.5	-1.0
			-1/2	-1	167.4	6.4	-0.8
				0	169.2	6.4	-0.4
				1	171.1	6.4	-0.5
			1/2	-1	189.8	6.4	-1.0
				0	191.6	6.4	-0.5
				1	193.4	6.4	0.1
			3/2	-1	212.0	6.4	-0.4
				0	213.7	6.4	0.7
				1	215.7	6.4	0.0
		-1/2 − 1/2	-3/2	-1	228.1	4.3	0.4
				0	229.8	4.3	1.0
				1	231.7	4.3	0.8
			-1/2	-1	244.7	4.3	-0.1
				0	246.3	4.3	1.0
				1	248.2	4.3	0.8
			1/2	-1	264.8	4.2	0.3
				0	266.6	4.2	0.5
				1	268.3	4.2	1.2
			3/2	-1	289.7	4.1	0.3
				0	291.5	4.1	0.6
				1	293.2	4.1	1.3
		-3/2 − -1/2	-3/2	0	441.1	2.1	-0.2
			-1/2	0	447.5	2.0	0.9
			1/2	0	460.1	2.0	0.3
			3/2	0	480.1	1.9	0.3
$4_{23} - 3_{12}$	7/2 − 7/2	-7/2 − -7/2	3/2	0	231.9	25.8	0.5
			1/2	0	236.1	25.8	-0.2
			-1/2	0	240.1	25.8	-1.7
			-3/2	0	243.7	25.8	0.4
			laser frequency = 1286.9995 GHz				
$3_{31} - 2_{20}$	5/2 − 5/2	5/2 − 5/2	-3/2	-1	1388.9	-19.8	-3.1
				0	1390.7	-19.8	-3.4
				1	1392.5	-19.8	-3.8
			-1/2	-1	1397.4	-19.8	-1.3
				0	1399.3	-19.8	0.2
				1	1401.1	-19.8	-0.1
			1/2	-1	1406.6	-19.7	-1.5
				0	1408.4	-19.7	-1.8
				1	1410.2	-19.7	-2.2
			3/2	-1	1416.6	-19.6	-1.4
				0	1418.4	-19.6	-1.7
				1	1420.2	-19.6	-2.1

TABLE 2—*Continued*

$N_{K_a K_c}$	J	M_J	$M_{I_{As}}$	M_{I_H}	flux density mT	tuning rate MHz/mT	obs - calc MHz
			laser frequency = 1302.8458 GHz				
		5/2 − 5/2	-3/2	-1	651.1	-22.9	0.9
				0	652.9	-22.9	0.7
				1	654.7	-22.9	0.3
			-1/2	-1	657.9	-22.9	0.0
				0	659.7	-22.9	-0.2
				1	661.5	-22.9	-0.6
			1/2	-1	665.5	-22.8	0.9
				0	667.3	-22.8	0.6
				1	669.0	-22.8	-2.1
			3/2	-1	673.7	-22.8	-1.4
				0	675.5	-22.8	-1.7
				1	677.3	-22.8	-2.1
		3/2 − 5/2	-3/2	-1	825.0	-17.1	1.9
				0	826.8	-17.1	1.5
				1	828.6	-17.1	1.1
			-1/2	-1	832.3	-17.1	1.4
				0	834.1	-17.1	1.2
				1	835.8	-17.1	-0.9
			1/2	-1	840.4	-17.0	-0.6
				0	842.2	-17.0	-0.9
				1	844.0	-17.0	-1.3
			3/2	-1	849.5	-17.0	-0.7
				0	851.3	-17.0	-1.2
				1	853.1	-17.0	-1.6
	2 − 1[a]	5/2 − 3/2	-3/2	-1	1107.0	-7.9	2.0
				0	1108.7	-7.9	0.7
				1	1110.6	-7.9	1.0
			-1/2	-1	1130.5	-7.5	1.5
				0	1132.3	-7.5	1.0
				1	1134.0	-7.5	-0.2
			1/2	-1	1155.6	-7.2	0.3
				0	1157.5	-7.2	0.5
				1	1159.3	-7.2	-0.0
			3/2	-1	1183.0	-6.8	0.9
				0	1184.7	-6.8	-0.3
				1	1186.5	-6.8	-0.8
			laser frequency = 1397.1186 GHz				
$3_{30} - 2_{21}$	7/2 − 5/2	5/2 − 5/2	3/2	0	1656.2	-11.3	-1.7
			1/2	0	1662.3	-11.3	-2.1
			-1/2	0	1667.4	-11.3	-3.3
			-3/2	0	1671.7	-11.4	-3.1
		3/2 − 5/2	3/2	0	1100.6	-13.4	-6.1[b]
			1/2	0	1104.0	-13.4	-7.4[b]
			-1/2	0	1107.5	-13.4	-7.2[b]
			-3/2	0	1110.9	-13.4	-8.1[b]
$6_{06} - 5_{15}$	1 − 1[a]	11/2 − 11/2	3/2	-1	1056.0	-25.0	0.3
				0	1057.7	-25.0	-0.6
				1	1059.4	-25.0	-1.5
			1/2	-1	1067.3	-24.9	0.2
				0	1069.1	-24.9	1.8
				1	1070.7	-24.9	-1.6
			-1/2	-1	1078.3	-24.7	-0.4
				0	1080.0	-24.7	-1.3
				1	1081.8	-24.7	0.2
			-3/2	-1	1089.1	-24.6	-1.2
				0	1090.9	-24.6	0.3
				1	1092.6	-24.6	-0.6
$6_{16} - 5_{05}$	1 − 1[a]	11/2 − 11/2	3/2	0	1057.7	-25.0	-1.2
			1/2	0	1069.0	-24.9	-1.3
			-1/2	0	1080.0	-24.7	-1.9
			-3/2	0	1090.9	-24.6	-0.2

TABLE 2—*Continued*

$N_{K_aK_c}$	J	M_J	$M_{I_{As}}$	M_{I_H}	flux density mT	tuning rate MHz/mT	obs - calc MHz
$7_{16} - 7_{07}$	15/2 − 13/2	5/2 − 3/2	-3/2	0	1499.4	-18.1	1.5
			-1/2	0	1508.0	-18.1	2.3
			1/2	0	1517.1	-18.2	0.9
			3/2	0	1526.8	-18.3	-0.4
	1 − 2[a]	5/2 − 7/2	-3/2	0	1655.9	-19.0	0.3
			-1/2	0	1663.9	-19.1	-1.4
			1/2	0	1672.1	-19.2	-1.2
			3/2	0	1680.6	-19.3	1.6
		7/2 − 5/2	-3/2	0	1745.0	-18.4	2.3
			-1/2	0	1753.7	-18.5	1.0
			1/2	0	1763.1	-18.6	0.7
			3/2	0	1773.2	-18.7	-1.1
$7_{26} - 7_{17}$	15/2 − 13/2	5/2 − 3/2	-3/2	-1	1497.6	-18.1	1.4
				0	1499.3	-18.1	-1.1
				1	1501.3	-18.1	1.9
			-1/2	-1	1506.2	-18.1	2.1
				0	1508.0	-18.1	1.5
				1	1509.8	-18.1	0.8
			1/2	-1	1515.3	-18.2	0.8
				0	1517.2	-18.2	2.0
				1	1519.0	-18.2	1.3
			3/2	-1	1524.9	-18.3	-2.4
				0	1526.9	-18.3	0.6
				1	1528.6	-18.3	-1.9
	1 − 2[a]	5/2 − 7/2	-3/2	-1	1654.0	-19.0	-1.8
				0	1655.8	-19.0	-2.4
				1	1657.7	-19.0	-1.2
			-1/2	-1	1662.2	-19.1	0.3
				0	1663.9	-19.1	-2.2
				1	1665.8	-19.1	-1.0
			1/2	-1	1670.3	-19.2	-1.5
				0	1672.1	-19.2	-2.1
				1	1674.1	-19.2	1.1
			3/2	-1	1678.8	-19.3	1.3
				0	1680.5	-19.3	-1.3
				1	1682.5	-19.3	2.0
		7/2 − 5/2	-3/2	-1	1743.1	-18.4	1.2
				0	1744.9	-18.4	0.5
				1	1746.9	-18.4	3.5
			-1/2	-1	1751.8	-18.5	-0.1
				0	1753.7	-18.5	1.0
				1	1755.5	-18.5	0.3
			1/2	-1	1761.3	-18.6	0.5
				0	1763.1	-18.6	-0.2
				1	1764.8	-18.6	-2.8
			3/2	-1	1771.4	-18.7	-1.3
				0	1773.2	-18.7	-2.0
				1	1775.1	-18.7	-0.9
		laser frequency = 1419.0493 GHz					
$5_{14} - 4_{23}$	11/2 − 9/2	-1/2 − -3/2	3/2	0	1250.4	1.9	-0.1
			1/2	0	1258.3	1.9	-0.2
			-1/2	0	1268.4	1.9	0.1
			-3/2	0	1280.7	1.9	1.1
		3/2 − 1/2	3/2	0	1610.4	1.5	-0.7
			1/2	0	1625.6	1.5	-0.3
			-1/2	0	1642.3	1.4	-0.1
			-3/2	0	1660.3	1.4	0.2
		5/2 − 3/2	3/2	0	1901.8	1.2	-0.3
			1/2	0	1922.3	1.1	-0.5
			-1/2	0	1943.1	1.1	-1.1
			-3/2	0	1962.8	1.1	-0.7
	9/2 − 7/2	7/2 − 7/2	-3/2	0	577.7	2.8	1.2
			-1/2	0	583.1	2.8	0.7
			1/2	0	589.3	2.8	0.3

TABLE 2—*Continued*

$N_{K_aK_c}$	J	M_J	$M_{I_{As}}$	M_{I_H}	flux density mT	tuning rate MHz/mT	obs - calc MHz
			3/2	0	596.1	2.8	0.5
		5/2 − 5/2	-3/2	0	901.3	1.5	-0.3
			-1/2	0	910.8	1.4	-0.1
			1/2	0	922.7	1.4	0.0
			3/2	0	936.7	1.4	0.2
		-1/2 − 1/2	3/2	0	512.7	2.4	-0.1
			1/2	0	520.5	2.5	0.0
			-1/2	0	529.5	2.5	-0.3
			-3/2	0	539.5	2.5	0.0
		-3/2 − -1/2	3/2	0	710.3	1.6	0.2
			1/2	0	725.1	1.6	0.4
			-1/2	0	740.6	1.5	0.3
			-3/2	0	756.8	1.5	0.1
$5_{24} - 4_{13}$	11/2 − 9/2	1/2 − -1/2	3/2	-1	1136.4	2.1	-0.3
				0	1138.0	2.1	0.0
				1	1139.9	2.1	-0.3
			1/2	-1	1144.9	2.1	0.4
				0	1146.7	2.1	0.3
				1	1148.4	2.1	0.4
			-1/2	-1	1155.5	2.1	0.5
				0	1157.3	2.1	0.4
				1	1159.1	2.1	0.3
			-3/2	-1	1167.9	2.0	1.0
				0	1169.8	2.0	0.7
				1	1171.5	2.0	0.8
		3/2 − 1/2	3/2	-1	1290.5	1.9	0.2[b]
				0	1292.4	1.9	-0.1
				1	1294.2	1.9	-0.3[b]
			1/2	-1	1302.4	1.9	0.4[b]
				0	1304.2	1.9	0.3
				1	1306.0	1.9	0.2[b]
			-1/2	-1	1315.8	1.9	0.2[b]
				0	1317.7	1.9	-0.1
				1	1319.3	1.9	0.2[b]
			-3/2	-1	1330.1	1.8	0.8[b]
				0	1332.1	1.8	0.3
				1	1333.9	1.8	0.2[b]
		5/2 − 3/2	3/2	-1	1495.6	1.7	-0.1[b]
				0	1497.6	1.7	-0.6
				1	1499.2	1.7	-0.4[b]
			1/2	-1	1511.1	1.7	-0.2[b]
				0	1512.9	1.7	-0.3
				1	1514.5	1.7	-0.1[b]
			-1/2	-1	1526.7	1.6	-0.1[b]
				0	1528.6	1.6	-0.4
				1	1530.2	1.6	-0.2[b]
			-3/2	-1	1542.5	1.6	-0.1[b]
				0	1544.2	1.6	0.0
				1	1546.0	1.6	-0.2[b]
		7/2 − 5/2	3/2	0	1784.7	1.4	-0.7
			1/2	0	1802.9	1.4	-0.8
			-1/2	0	1819.4	1.4	-0.7
			-3/2	0	1833.9	1.4	-0.3
	9/2 − 7/2	-5/2 − -3/2	3/2	0	183.7	1.4	-1.3
			1/2	0	209.9	1.5	-1.2
			-1/2	0	235.3	1.5	-1.1
			-3/2	0	259.5	1.5	-0.6
		-7/2 − -5/2	3/2	0	295.8	0.8	-1.3
			1/2	0	345.0	0.8	-1.0
			-1/2	0	392.1	0.8	-0.9
			-3/2	0	436.4	0.8	-1.1
$6_{06} - 5_{15}$	11/2 − 11/2	11/2 − 11/2	3/2	-1	485.8	-17.9	3.1
				0	487.5	-17.9	3.6
				1	489.0	-17.9	0.5
			1/2	-1	511.9	-17.2	1.8
				0	513.6	-17.2	2.4
				1	515.3	-17.2	2.8

TABLE 2—*Continued*

$N_{K_aK_c}$	J	M_J	$M_{I_{As}}$	M_{I_H}	flux density mT	tuning rate MHz/mT	obs - calc MHz
			-1/2	-1	538.1	-16.6	1.0
				0	539.8	-16.6	1.5
				1	541.3	-16.7	-1.3
			-3/2	-1	564.4	-16.1	0.4
				0	566.0	-16.1	-0.5
				1	567.6	-16.2	-1.6
$6_{16} - 5_{05}$	11/2 − 11/2	11/2 − 11/2	3/2	0	487.4	-17.9	1.2
			1/2	0	513.6	-17.2	1.8
			-1/2	0	539.7	-16.6	-0.7
			-3/2	0	566.0	-16.1	-1.1
		laser frequency = 1626.6026 GHz					
$5_{23} - 4_{32}$	$1 - 1^a$	9/2 − 9/2	-3/2	0	840.7	-4.6	-1.3
			-1/2	0	844.6	-4.6	-1.1
			1/2	0	849.5	-4.7	-1.3
			3/2	0	855.6	-4.7	-1.0
		7/2 − 7/2	-3/2	0	1128.1	-3.1	-0.7
			-1/2	0	1134.0	-3.1	-0.7
			1/2	0	1140.7	-3.1	-0.9
			3/2	0	1148.3	-3.1	-0.9
		5/2 − 5/2	-3/2	0	1793.4	-1.5	1.4
			-1/2	0	1806.5	-1.4	1.1
			1/2	0	1820.2	-1.4	0.8
			3/2	0	1834.7	-1.4	0.6
		laser frequency = 1726.5485 GHz					
$3_{31} - 2_{02}$	$2 - 2^a$	3/2 − 3/2	-3/2	-1	1122.9	-13.3	1.9
				0	1124.8	-13.3	2.7
				1	1126.6	-13.3	2.1
			-1/2	-1	1136.1	-13.3	3.0
				0	1137.9	-13.3	2.5
				1	1139.7	-13.3	1.9
			1/2	-1	1149.3	-13.4	0.5
				0	1151.2	-13.4	1.4
				1	1153.0	-13.4	0.8
			3/2	-1	1163.1	-13.4	1.0
				0	1165.0	-13.4	1.8
				1	1166.9	-13.4	2.6
		1/2 − 1/2	-3/2	-1	1248.1	-9.3	2.8
				0	1249.9	-9.3	2.4
				1	1251.7	-9.3	1.9
			-1/2	-1	1260.5	-9.3	2.0
				0	1262.4	-9.3	2.5
				1	1264.2	-9.3	2.0
			1/2	-1	1274.2	-9.3	1.2
				0	1276.0	-9.3	0.7
				1	1277.9	-9.3	1.2
			3/2	-1	1289.2	-9.2	1.0
				0	1291.0	-9.2	0.6
				1	1292.9	-9.2	1.0
$4_{41} - 3_{30}$	7/2 − 5/2	1/2 − 3/2	-3/2	0	1074.7	3.0	-0.3
			-1/2	0	1100.6	3.0	-0.7
			1/2	0	1128.5	2.9	-1.2
			3/2	0	1158.2	2.8	-0.8

festation of the negligible asymmetry doubling for these high K_c levels.

Analysis

The measurements in Table 2 were used to determine the parameters of an effective Hamiltonian for an asymmetric rotor

$$H_{\text{eff}} = H_{\text{rot}} + H_{\text{cd}} + H_{\text{fs}} + H_{\text{hfs}} + H_{\text{Q}} + H_{\text{Zeem}} \qquad [1]$$

as formulated by Bowater *et al.* (*14*). The centrifugal distortion corrections to the rotational and spin–rotational Hamiltonians were included in the asymmetric (*A*) reduction forms of Watson (*15*) and Brown and Sears (*16*). Despite the fact that

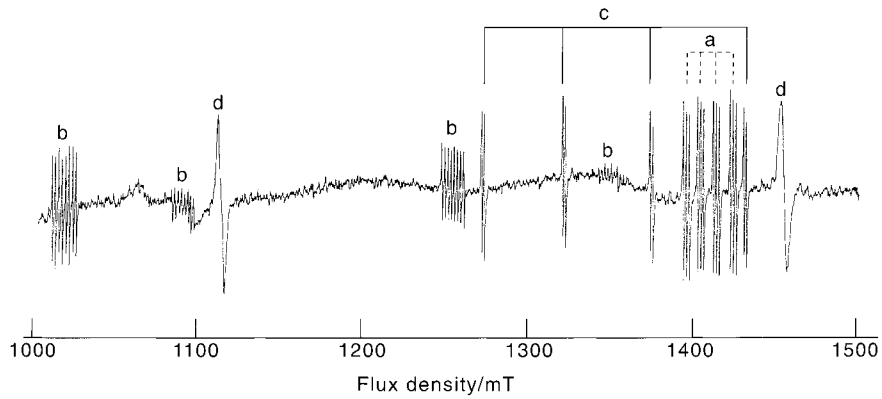

FIG. 2. Part of the LMR spectrum of the reaction products of F + AsH_2 recorded using the 232.9-μm laser line of CH_3OH, pumped by 9R10 of CO_2 in parallel polarization. *a:* AsH_2 (*ortho*) in its ground state; *b:* AsH in its ground $^3\Sigma^-$ state; *c:* AsH in its first excited $^1\Delta$ state; *d:* NH_2 in its ground state. Note that the experimental conditions used in this recording were not optimized for production of AsH_2 compared with AsH. Increase of the AsH_3 flow rate promotes the formation of the former over the latter.

the inertial properties of AsH_2 are accidentally very close to those of an oblate symmetric top, we have chosen to use a I^r representation (*15*) because this makes comparison with other workers more straightforward. The FIR data (comprising 27 rotational transitions) were fitted, together with the six rotational transitions observed in the millimeter study (*8*), by a linearized, least-squares procedure. This was carried out using a computer program based on the Bowater *et al.* paper (*14, 17, 18*) and modified for (i) two nuclear spins, (ii) the inclusion of nuclear spin–rotation parameters, (iii) the option of using a decoupled basis set,[5] and (iv) an alternative method of eigenvalue identification. A decoupled labeling scheme $|N, S, J, M_J, I_1, M_{I_1}, I_2, M_{I_2}\rangle$ was used for the FIR data and a coupled scheme $|N, S, J, I_1, F_1, I_2, F\rangle$ for the millimeter-wave data, where $\mathbf{F}_1 = \mathbf{J} + \mathbf{I}_1$ (not to be confused with the F_1 spin component) and $\mathbf{F} = \mathbf{F}_1 + \mathbf{I}_2$. The matrix representation of H_{eff} was truncated at $\Delta N = 2$ and $\Delta K_a = 6$, except for transitions with $N = 7$ for which $\Delta K_a = 8$, without loss in accuracy. FIR measurements were given uncertainties of 2 MHz unless overlapped, in which case they were given uncertainties equivalent to zero weight. The millimeter data were given uncertainties of 0.03 or 0.1 MHz, or zero weight, in accordance with the weights given in Ref. (*8*). The final choice of parameters included in the fit was arrived at by trial and error. Each of the higher order parameters which was selected not only improved the overall quality of fit but was also reasonably well determined (with a standard deviation at least four times smaller than the magnitude of the parameter). No attempt was made to include centrifugal distortion corrections to the nuclear hyperfine parameters because the hyperfine splittings were well-fitted without them. The residuals of the FIR data in the fit are given in Table 2. The quality of fit of the millimeter-wave data was similar to that given in Ref. (*8*). The parameters determined in the fit are given in Table 3 in megahertz, and also in reciprocal centimeters for convenience, together with the values of the millimeter-wave parameters (*8*) for comparison. It can be seen in Table 3 that the level of agreement between the rotational and spin–rotational parameters from the two studies is really rather poor. The reason for this is that Fujiwara *et al.* (*8*) worked with a restricted data set and had to assume values for several of the centrifugal distortion parameters. The assumed values were not always very good, e.g., Δ_K^S was con-

[5] Decoupled matrix elements may be obtained from the corresponding expressions for coupled matrix elements by replacing

$$\delta_{M_F' M_F}\delta_{F'F}(-1)^{J+I+F}\begin{Bmatrix} I & J' & F \\ J & I & k \end{Bmatrix} \text{ with}$$

$$\sum_p (-1)^p (-1)^{I-M_I'}\begin{pmatrix} I & k & I \\ -M_I' & -p & M_I \end{pmatrix}(-1)^{J'-M_J'}\begin{pmatrix} J' & k & J \\ -M_J' & p & M_J \end{pmatrix},$$

where k is the rank of the spherical tensor operator involved.

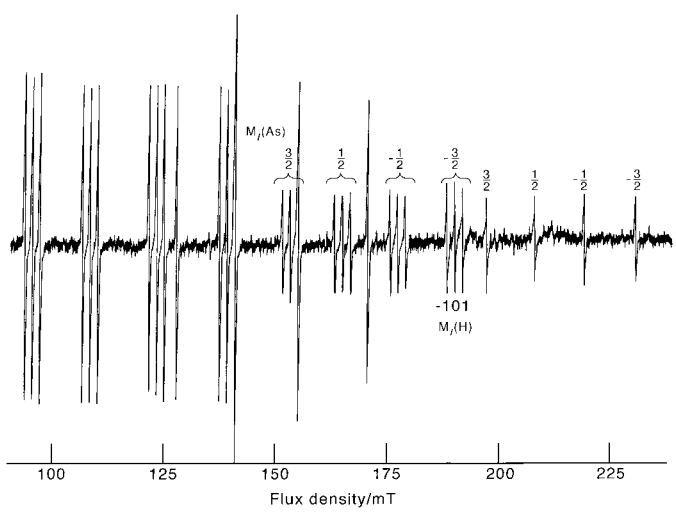

FIG. 3. Part of the LMR spectrum of AsH_2 recorded using the 382.636-μm laser line of CH_2F_2, pumped by 9R10″ of CO_2 in parallel polarization. $N_{K_aK_c}$, $F_i = 3_{13}$–2_{20}, F_2–F_1 (*ortho*), and 3_{03}–2_{12}, F_2–F_1 (*para*). $M_J = -\frac{5}{2}$–$(-\frac{5}{2})$ (stronger signals), $-\frac{3}{2}$–$(-\frac{3}{2})$ (weaker signals).

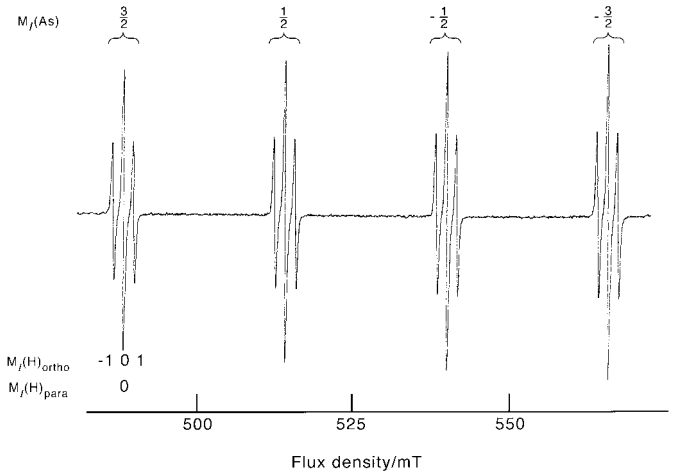

FIG. 4. Part of the LMR spectrum of AsH_2 recorded using the 211.261-μm laser line of CH_3OH, pumped by 9R32 of CO_2 in parallel polarization. $N_{K_aK_c}$, $F_i = 6_{06}$–5_{15}, F_2–F_1 (*ortho*), and 6_{16}–5_{05}, F_2–F_1 (*para*). $M_J = \frac{11}{2}$–$\frac{11}{2}$. The 1:2:1 hyperfine pattern arises from the overlap of the singlet (*ortho*) and triplet (*para*) patterns. At higher resolution, this central line would be split by the effects of *K*-type doubling of the proton hyperfine parameter ab_I(H) which mixes *ortho* and *para* states directly.

strained to be 15.59 MHz, whereas its true value is now determined as 25.53 MHz. The effects of these choices were absorbed into the other parameters, thereby distorting them. Because we have been able to fit a very much larger data set in the present work (608 resonances compared with 61 in the millimeter-wave study), our parameter set is significantly more accurate.

Table 4 compares the current values of the molecular parameters with the optical values of Ref. (*2*), while term values in reciprocal centimeters calculated from the current and optical parameters are shown in Table 5. The parameters which are determined for the first time in the present work include the *g* factors, the sextic centrifugal distortion parameters, and some of the quartic centrifugal distortion parameters and centrifugal distortion corrections to spin–rotation parameters.

DISCUSSION

Rotational Parameters

The refined rotational parameters can be used to determine an improved geometry for AsH_2. The zero-point geometry is best determined from A_0 and B_0 because these two parameters are not affected by Coriolis coupling, unlike C_0. The results of the calculation are r_0 (As–H) = 1.518 Å, θ_0 (H–As–H) = 90.746°. A more sophisticated treatment of the geometry of AsH_2 can be found in Ref. (*8*). The bond angle θ decreases down the Group V dihydrides, with $\theta = 103.33°$ for NH_2 (*19*) and 91.65° for PH_2 (*20*). By inserting the values of the rotational parameters into the expression for the asymmetry parameter $\kappa = (2B_0 - A_0 - C_0)/(A_0 - C_0)$, it can be seen that AsH_2 is a near-symmetric oblate top with κ equal to 0.8. This value compares with −0.3 and 0.6 for NH_2 and PH_2, respectively. While AsH_2 and PH_2 have similar bond angles, AsH_2 is closer to the oblate symmetric top limit because the center of mass is closer to the central atom in the heavier molecule. The near symmetry of AsH_2 arises "accidentally" as a result of the near-90° bond angle causing the moments of inertia about the in-plane *a* and *b* axes to be nearly equal. This is in contrast to "real" cases of symmetry which are due to the equivalence of bonds. A consequence of near symmetry is that the K_c asymmetry doubling is less pronounced in AsH_2 than in a more asymmetric molecule like PH_2.

Centrifugal Distortion Parameters

The full set of quartic centrifugal distortion parameters Δ_N, Δ_{NK}, Δ_K, δ_N, and δ_K have been determined and can be used to calculate the force field of AsH_2 from which the symmetric and asymmetric stretching (ν_1, ν_3) and bending (ν_2) vibrational frequencies can be estimated (*9, 21*). While all three vibrational frequencies have been calculated by *ab initio* methods (*11*), only ν_2 has been determined experimentally, and even then only approximately (*4*). The three sextic centrifugal distortion parameters, Φ_{KN}, ϕ_N, and ϕ_K, which have been determined, help to improve the reliability of the quartic centrifugal distortion parameters. The values of the quartic centrifugal parameters determined in this work agree tolerably well with those predicted by the force field given in Ref. (*9*) ($\Delta_N = 13.93$ MHz, $\Delta_{NK} = -45.801$ MHz, $\Delta_K = 66.427$ MHz, $\delta_N = 6.25$ MHz, and $\delta_K = -5.7697$ MHz).

Spin–Rotation Parameters

The spin–rotation parameters give an indication of the contamination of the ground electronic state of AsH_2 by excited electronic states. The dominant contribution to the effective spin–rotation interaction is expected to be second order, via spin–orbit coupling (*22*). This is also the case for the anisotropic corrections to the electron spin *g* factors, g_s^{ii} (*23*). Inserting the determined parameter values into Curl's relationship,

$$-\epsilon_{ii}/2B_{ii} = g_s^{ii} - g_s,^6 \qquad [2]$$

which is based on the assumption that the second-order contributions are dominant, it can be seen that for AsH_2 this assumption is valid as is shown in Table 6.

While the rotational parameters show oblate character with A_0 and B_0 being nearly equal, the spin–rotation parameters are more asymmetric in character with ϵ_{aa} nearly three times the size of ϵ_{bb}. This can be explained by the particular excited states with which the ground state must mix in order to give a

[6] g_s has a value of 2.0020 and is the isotropic value of the *g* factor, corrected from the free-electron value to take account of relativistic effects.

TABLE 3

Molecular Parameters Determined for AsH_2 in the $v = 0$ Level of its Ground $^2B_1$ State

Parameter	Present work/cm^{-1}	Present work/MHz	Submillimetre-wave/MHz [8]
A	7.54966748(57)[a]	226333.337(17)	226347.254(31)
B	7.16288840(57)	214737.992(17)	214738.272(9)
C	3.6149040(10)	108372.098(31)	108369.402(10)
Δ_N	0.472747(73) x 10^{-3}	14.1726(22)	12.57[b]
Δ_{NK}	-0.156762(43) x 10^{-2}	-46.996(13)	-31.366(18)
Δ_K	0.227070(47) x 10^{-2}	68.074(14)	54.050(14)
δ_N	0.215005(67) x 10^{-3}	6.4457(20)	5.59[b]
δ_K	-0.13793(19) x 10^{-3}	-4.1351(58)	-2.8638(7)
Φ_{KN}	0.5627(47) x 10^{-6}	0.1687(14) x 10^{-1}	
ϕ_N	-0.55(13) x 10^{-8}	-0.166(38) x 10^{-3}	
ϕ_K	0.571(17) x 10^{-6}	0.1713(50) x 10^{-1}	
ϵ_{aa}	-1.1051846(37)	-33132.60(11)	-33088.39(10)
ϵ_{bb}	-0.3950230(24)	-11842.493(73)	-11858.45(7)
ϵ_{cc}	0.42713(24) x 10^{-2}	128.050(73)	89.60(6)
Δ_K^S	0.8516(57) x 10^{-3}	25.53(17)	15.59[b]
$\Delta_{NK}^S + \Delta_{KN}^S$	-0.3312(60) x 10^{-3}	-9.93(18)	
Δ_{NK}^S	0.0[b]	0.0[b]	-4.93[b]
Δ_{KN}^S			-7.385(24)
Δ_N^S	0.8126(93) x 10^{-4}	2.436(28)	2.63[b]
δ_K^S	0.3559(67) x 10^{-4}	1.067(20)	
δ_N^S	0.4240(47) x 10^{-4}	1.271(14)	
a_F(As)	0.192875(37) x 10^{-2}	57.823(11)	57.820(7)
aa_I(As)	-0.959657(63) x 10^{-2}	-287.698(19)	-287.694(24)
bb_I(As)	-0.1074600(47) x 10^{-1}	-322.157(14)	-322.150(15)
aa_Q(As)	0.17334(24) x 10^{-3}	5.1967(72)	5.202(9)
bb_Q(As)	-0.78364(24) x 10^{-3}	-23.4928(71)	-23.480(9)
C_{aa}(As)	0.2245(17) x 10^{-4}	0.6731(50)	0.672(6)
C_{bb}(As)	0.1613(16) x 10^{-4}	0.4837(49)	0.471(7)
C_{cc}(As)	0.414(16) x 10^{-5}	0.1240(49)	0.125(5)
a_F(H)	-0.169451(47) x 10^{-2}	-50.800(14)	-50.811(18)
aa_I(H)	-0.285(17) x 10^{-4}	-0.855(50)	-0.81(6)
bb_I(H)	-0.1036(11) x 10^{-3}	-3.107(32)	-3.13(4)
g_{aa}^s	2.072895(69)		
g_{bb}^s	2.027805(58)		
g_{cc}^s	1.999932(58)		
g_{aa}^r	-0.981(21) x 10^{-3}		
g_{bb}^r	-0.251(15) x 10^{-3}		
g_{cc}^r	-0.18(15) x 10^{-4}		
g_N(As)	0.95965[c]		
g_N(H)	5.58569[c]		

[a] The numbers in parentheses correspond to one standard deviation of the least-squares fit.

[b] Parameters constrained to this value in the least-squares fit (see text).

[c] Nuclear g factors for ^{75}As and ^{1}H (fixed) (*32*).

nonzero spin–orbit interaction. For rotation about the a axis, it can be shown that the relevant excited state must have A_1 orbital symmetry, which is the symmetry of the first excited state of AsH_2 (*1, 2*). For rotation about the other axes, the appropriate symmetries are those of higher excited states, ϵ_{bb} and ϵ_{cc} arising from admixture of the ground state with $^2B_2$ and $^2A_2$ states, respectively. Therefore, the largest second-order contribution to the spin–rotation parameters occurs for ϵ_{aa} because mixing between the ground and first excited states is greater than the mixing between the ground and higher excited states. The $\tilde{A}^2A_1$ and $\tilde{X}^2B_1$ states would form a degenerate $^2\Pi$ state if AsH_2 were linear; in reality, they are split apart by the Renner–Teller interaction (*24*). This correlation shows the connection between spin–orbit coupling in the linear molecule and the effective spin–rotation coupling about the a-inertial axis in the bent molecule. A simple calculation, based on the second-order formula given by Dixon (*25*) with the additional assumption that the X and A states are related by the promotion of an unpaired electron from the out-of-plane to an in-plane $4p$ orbital on the As atom, provides an estimate for ϵ_{aa} of -1.8 cm^{-1}.

Five of the six quartic centrifugal distortion corrections to the spin–rotation parameters (*16*), namely Δ_K^S, $\Delta_{NK}^S + \Delta_{KN}^S$, Δ_N, δ_K^S, and δ_N^S, have been determined and considerably improve

TABLE 4
Comparison of the Parameters Determined in the Optical and FIR Studies

Parameter	Optical[a]	Optical[b]	FIR
A_0	7.5486(43)	7.5506(59)	7.5467528(57)
B_0	7.1624(45)	7.1593(63)	7.1628915(60)
C_0	3.6166(30)	3.624(18)	3.6149003(11)
$10^3\Delta_N$	0.4193[a]	0.49(11)	0.473011(77)
$10^2\Delta_{NK}$	-0.1328	-0.136(20)	-0.156902(47)
$10^2\Delta_K$	0.2023		0.227251(50)
$10^3\delta_N$	0.1866		0.215069(67)
$10^3\delta_K$	-0.1672		-0.13689(20)
ϵ_{aa}	-1.050(23)	-1.031(47)	-1.1051899(37)
ϵ_{bb}	-0.399(25)	-0.341(40)	-0.3950044(25)
$10^2\epsilon_{cc}$	0.5(27)	0.024(40)	0.42546(25)

[a] Parameter values taken from Ref. (*2*). The five centrifugal distortion parameters were calculated from the four τ parameters given in Ref. (*2*): $\tau_{aaaa} = -0.00446(34)$, $\tau_{bbbb} = -0.00317(45)$, $\tau_{aabb} = 0.00219(86)$ and $\tau_{abab} = -0.00057(42)$ cm^{-1}.
[b] Determined from a re-fit of the combination differences of Ref. (*2*).

the reliability of the spin–rotation parameters. Since the sixth parameter, Δ_{NK}^S, was only poorly determined, it was constrained to zero in the final fit.

Nuclear Hyperfine Parameters

Although the present fit has improved the precision of the hyperfine parameters (see Table 3), the values are essentially the same as those determined in the millimeter-wave study (*8*), where a quantitative discussion of the hyperfine parameters for arsenic is given. Consequently only a brief discussion is provided here.

Fermi-contact parameters. The Fermi-contact parameter is a measure of the unpaired electron density at the nucleus and as such it gives an indication of the *s* character of the orbital containing the unpaired electron. At the most simplistic level, the unpaired electron in AsH_2 occupies a b_1 orbital (which might be approximated by a 4*p* orbital on the arsenic atom). In this case, one would expect the Fermi-contact interaction to be zero at both the As and H nuclei. In reality, the parameter is small but nonzero at each nucleus. Using the values for the Fermi-contact interaction in a pure *ns* orbital (*26*), the *s* character of the orbital which contains the unpaired electron in AsH_2 can be determined. The Fermi-contact parameters at the ^{75}As and ^{1}H nuclei, given in Table 3, imply that the spin densities at these nuclei are 0.39 and −3.6%, respectively. The signs of these two quantities are as expected if the nonzero spin density arises from spin polarization in the As–H σ bond.

Spin–spin dipolar parameters. The dipolar hyperfine parameters depend on the spatial distribution of the unpaired electron spin in the molecule. For the ^{75}As nucleus, the out-of-plane component is large, positive, and roughly twice the magnitude of the two in-plane components. This is in line with the expectation that the unpaired electron is in a 4*p* atomic orbital on the As atom. Fujiwara *et al.* (*8*) have calculated that, on this basis, the unpaired spin density on the As atom is expected to be 91.4%, suggesting some contribution to the b_1 orbital from the hydrogen orbitals. The spin density on the

TABLE 5
Computed Term Values in cm^{-1} for AsH_2 in the $v = 0$ of the $\tilde{X}^2B_1$ Ground State

		F_1^c			F_2^d	
$N_{K_aK_c}$	optical[a]	FIR[b]	diff	optical	FIR	diff
1_{01}	10.70	10.6773	0.02	10.94	10.9711	0.03
1_{11}	10.92	10.8812	0.04	11.68	11.7144	0.03
1_{10}	14.36	14.3299	0.03	15.39	15.4607	0.07
2_{02}	28.96	28.8930	0.07	29.45	29.4707	0.02
2_{12}	28.98	28.9142	0.07	29.53	29.5462	0.02
2_{11}	39.39	39.3462	0.04	40.39	40.4765	0.09
2_{21}	40.21	40.1456	0.06	42.08	42.1625	0.38
2_{20}	43.43	43.3750	0.06	45.20	45.2995	0.10
3_{03}	54.40	54.2856	0.11	54.93	54.9240	0.01
3_{13}	54.40	54.2873	0.11	54.94	54.9295	0.01
3_{12}	72.48	72.3895	0.09	73.92	73.9995	0.08
3_{22}	72.61	72.5150	0.10	74.21	74.2903	0.08
3_{21}	82.60	82.5393	0.06	84.23	84.3547	0.12
3_{31}	84.41	84.3135	0.10	87.24	87.3606	0.12
3_{30}	87.22	87.1418	0.08	89.78	89.9180	0.14
4_{04}	87.08	86.9015	0.18	87.61	87.5620	0.05
4_{14}	87.08	86.9017	0.18	87.61	87.5627	0.05
4_{13}	112.58	112.4465	0.13	114.19	114.2558	0.07
4_{23}	112.59	112.4604	0.13	114.23	114.2879	0.06
4_{22}	130.54	130.4332	0.11	132.69	132.8190	0.13
4_{32}	130.95	130.8390	0.11	133.44	133.5776	0.14
4_{31}	140.28	140.2092	0.07	142.52	142.6917	0.17
4_{41}	143.44	143.3202	0.12	147.21	147.3647	0.15
4_{40}	145.75	145.6519	0.10	149.18	149.3477	0.17
5_{05}	126.97	126.7383	0.23	127.49	127.4122	0.01
5_{15}	126.97	126.7383	0.23	127.49	127.4122	0.01
5_{14}	159.85	159.6789	0.17	161.53	161.5750	0.05
5_{24}	159.85	159.6805	0.17	161.53	161.5783	0.05
5_{23}	185.33	185.1960	0.13	187.83	187.9522	0.12
5_{33}	185.39	185.2556	0.13	187.94	188.0676	0.87
5_{32}	202.95	202.8443	0.11	205.70	205.8721	0.17
5_{42}	203.92	203.8164	0.10	207.27	207.4569	0.19
5_{41}	212.40	212.3281	0.07	215.28	215.4958	0.22
5_{51}	217.24	217.1046	0.14	221.96	222.1358	0.82
5_{50}	219.03	218.9189	0.05	223.40	223.5980	0.20
6_{06}	174.07	173.7886	0.28	174.58	174.4718	0.11
6_{16}	174.07	173.7886	0.28	174.58	174.4718	0.11
6_{15}	214.32	214.1162	0.20	216.03	216.0676	0.23
6_{25}	214.32	214.1163	0.20	216.03	216.0680	0.23
6_{24}	247.16	247.0060	0.15	249.80	249.9334	0.13
6_{34}	247.16	247.0141	0.15	249.81	249.9487	0.14
6_{33}	272.49	272.3709	0.12	275.75	275.9380	0.19
6_{43}	272.67	272.5561	0.11	276.06	276.2570	0.20
6_{42}	289.57	289.4864	0.10	292.84	293.0646	0.78
6_{52}	291.49	291.3965	0.09	291.49	295.9147	0.42
6_{51}	298.95	298.8770	0.07	302.50	302.7712	0.27
6_{61}	305.72	305.5898	0.13	311.39	311.6012	0.21
6_{60}	307.04	306.9316	0.11	312.41	312.6347	0.22
7_{07}	228.35	228.0445	0.31	228.85	228.7348	0.12
7_{17}	228.35	228.0445	0.31	228.85	228.7348	0.12
7_{16}	275.96	275.7511	0.21	277.69	277.7432	0.05
7_{26}	275.96	275.7511	0.21	277.69	277.7432	0.05
7_{25}	316.12	315.9760	0.14	318.85	319.0105	0.85
7_{35}	316.12	315.9771	0.14	318.85	319.0125	0.84
7_{34}	348.83	348.7263	0.10	352.34	352.5647	0.22
7_{44}	348.86	348.7571	0.10	352.39	352.6172	0.23
7_{43}	373.89	373.8005	0.09	377.81	378.0650	0.75
7_{53}	374.35	374.2699	0.08	378.53	378.8060	0.28
7_{52}	390.26	390.1781	0.08	394.05	394.3186	0.27
7_{62}	393.57	393.5253	0.04	398.58	398.9132	0.33
7_{61}	399.90	399.8505	0.05	404.20	404.5311	0.33
7_{71}	408.77	408.6803	0.09	415.40	415.6628	0.26
7_{70}	409.71	409.6337	0.08	416.10	416.3712	0.27

[a] Calculated from the parameters determined from a fit of the combination differences of Ref. (*2*), see Table 4.
[b] Calculated from the parameters determined in the present study.
[c] $J = N + \frac{1}{2}$
[d] $J = N - \frac{1}{2}$

TABLE 6
A Test of Curl's Relationship for AsH_2

i	$-\epsilon_{ii}/2B_{ii}$	$g_s^{ii} - g_s$
a	0.073	0.071
b	0.028	0.026
c	-0.00059	-0.0021

heavy atom increases down the Group V dihydrides (*8*), consistent with the increase in size of the *np* orbital and a consequent decrease in the overlap with 2*p* orbitals on the H atoms.

One interesting characteristic of the ^{75}As dipolar parameters is that the two in-plane components aa_I and bb_I, though close, are not equal to each other. This is an indication that the electron spin density is not cylindrically symmetric about the *c* inertial axis but rather bulges out in the *b*-axis direction. Indeed, the same characteristic is shown by NH_2 and PH_2 (*8*), though it becomes more noticeable as one goes down Group V. It is not possible to explain this by admixture of higher *l* orbitals into the basic 4*p* component of the b_1 orbital because neither NH_2 or PH_2 have access to *f* orbitals. Equally, an explanation in terms of participation of 2*p* orbitals on the H atoms is not convincing because such participation gets smaller down the group (because of smaller overlap and increasing bond lengths), not larger. The noncylindrical symmetry of the dipolar tensor does seem to be reproduced by *ab initio* calculations (*27, 28*), but the physical explanation for this behavior is not considered in these papers.

The dipolar hyperfine parameters for the protons in AsH_2 have also been determined (see Table 3). We have attempted a simple interpretation of these parameters by modeling the b_1 orbital with a 4*p* Slater-type orbital on the arsenic atom. The results of the calculation are given in Table 7, after transformation into the principal axis system. The results obtained are of the correct general magnitude but somewhat smaller than those determined by experiment. This can be seen as a satisfactory result, given that the dipolar tensor components will also be affected by spin-polarization effects similar to those which contribute to the Fermi-contact interaction (see above).

Electric quadrupole parameters. The electron quadrupole coupling parameters for ^{75}As depend on the electric field gradients at the nucleus which are produced by all nearby charges, not just the open-shell electrons. Fujiwara *et al.* (*8*) have followed a standard treatment of this interaction (*31*) based on sp^n hybrid orbitals on the As atom. These orbitals are combinations of 4*s* and 4*p* atomic orbitals. They used the experimental values for $\alpha\alpha_Q$ to determine the *s* character of the σ orbitals which are used to form the As–H bonds. Their result is that the square of the coefficient a_s^2 is 0.118, which would correspond to a bond angle of 97.7° within the terms of this simple model. This result is not entirely satisfactory because the bond angle in AsH_2 is known to be 90.75°, very nearly a right angle. In other words, the bonding in AsH_2 can be more convincingly discussed in terms of $4p_x$ and $4p_y$ orbitals directed along the two As–H bond directions, with the lone pair accommodated in a 4*s* orbital. We have therefore repeated the calculation described in Ref. (*8*) with the difference that we take a_s^2 to be 0.0133, corresponding to the experimental bond angle of 90.75°, and we also place a full single electron in the $4p_z(b_1)$ orbital rather than 0.914 as do Fujiwara *et al.* (the latter made their estimate of the spin density in the b_1 orbital on the assumption that it was a 4*p* atomic orbital; this is almost certainly not a reliable assumption). The results of this calculation, compared with the experimental values for the electric quadrupole coupling parameters, are given in Table 8. It can be seen that the agreement is poor: indeed, the results of the calculation depend very strongly on the precise choice of value for a_s^2. In other words, the interaction depends sensitively on the charge distribution around the ^{75}As nucleus and much better agreement could be obtained by distorting the 4*p* and 4*s* orbitals. We have already seen that such distortion is required to explain the experimental dipole–dipole parameters. For the in-plane, bonding orbitals (a_1), this distortion might be modeled by inclusion of 4*d* character.

TABLE 7
Comparison of Experimental, Theoretical, and Estimated Dipolar Hyperfine Parameters for ^1H

	Parameter	Experimental[b]	Theoretical[c]	Estimated[d]
NH_2	aa_I	18.4	17.4	20.6
	bb_I	-13.2	-9.5	-6.3
	cc_I	-5.1	-8.0	-14.3
	ab_I	58.5	-56.7	-56.8
PH_2	aa_I	-1.0	-0.7	0.3
	bb_I	-4.4	-1.4	-0.7
	cc_I	5.5	2.4	0.4
	ab_I		-16.9	-16.3
AsH_2	aa_I	-0.9		-0.0
	bb_I	-3.1		-0.4
	cc_I	4.0		0.4
	ab_I			-13.5

[a] Values in MHz.
[b] Refs. (*29*) (NH_2) and (*30*) (PH_2).
[c] Refs. (*27*) (NH_2) and (*28*) (PH_2).
[d] Estimate based on an unpaired electron in an out-of-plane *np* orbital on the heavy atom (see text).

TABLE 8
Comparison of Experimental and Calculated Electric Quadrupole Parameters ii_Q for ^{75}As

	Experimental value	Estimated value[b]
aa_Q	5.2.	0.5.
bb_Q	-23.5.	-2.8.

[a] Values in MHz.
[b] Estimate based on hybrid sp^n orbitals, constructed to reproduce the experimental bond angle (see text).

TABLE 9

Comparison of Experimental and Calculated[a] Rotational g Factors for ^{75}As

i	$10^3 g_{r(\mathrm{exp})}^{ii}$	$10^3 g_{r_{\mathrm{elec}}(\mathrm{calc})}^{ii}$
a	-0.99	-0.74
b	-0.26	-0.26
c	-0.021	-0.0028

[a] $g_{r_{\mathrm{elec}}}^{ii} = -|\epsilon_{ii}|/\zeta_{4p}$.

Nuclear spin–rotation. As with the electron spin–rotation parameters discussed earlier, the main contribution to the nuclear spin–rotation parameters is expected to be from spin–orbit coupling in second order. This is found to be the case as the values determined for ^{75}As agree to within an order of magnitude with values calculated from the second-order perturbation theory expression (*8*). The nuclear spin–rotation parameters for AsH_2 are similar to that of AsH but both are larger than those of AsH_3. This can be explained by the facts that the separation between the ground and first excited electronic states is larger for AsH_3 and the rotational parameters themselves are smaller.

g Factors

The electron spin g factors g_s have been discussed above in connection with the spin–rotation parameters. The mean value of the three experimentally determined g_s^{ii} parameters (see Table 3) is 2.0335. This is in good agreement with the value of g_{av} (2.034) obtained in the EPR study of AsH_2 in a matrix (*5*).

The rotational g factors contain contributions from rotation of the nuclei (g_r^n) and electrons (g_r^e): $g_r = g_r^n - g_r^e$. As is usual for open-shell molecules, the electronic contribution outweighs the nuclear contribution resulting in negative values of g_r. The determined values agree well with values of the electronic contribution calculated from the expression $g_{r_{\mathrm{elec}}} = -|\epsilon_{ii}|/\zeta_{4p}$ with $\zeta_{4p} = 1201$ cm^{-1} (*33*)[7] (see Table 9).

CONCLUSION

A comprehensive study of the rotational spectrum of the AsH_2 free radical has been made by far-infrared laser magnetic resonance. A good spread of N and K_c values is involved in this study, as a result of which it has been possible to determine a much more reliable set of parameters than previously. The molecule can now be considered to be well characterized in the zero-point level of its ground electronic state.

[7] ζ_{4p} is the theoretical spin–orbit coupling constant for the As atom. It is consistent with the estimated value of 1250 cm^{-1} given in (*2*).

ACKNOWLEDGMENTS

We are very grateful to Professor Shuji Saito for several discussions of the AsH_2 problem and for providing copies of his papers (*8, 9*) before publication. R.A.H. thanks Jesus College, Oxford and the Physical and Theoretical Chemistry Laboratory for financial support.

REFERENCES

1. R. N. Dixon, G. Duxbury, and H. M. Lamberton, *Chem. Commun. (London)* **14,** 460–461 (1966).
2. R. N. Dixon, G. Duxbury, and H. M. Lamberton, *Proc. Roy. Soc.* **305,** 271–289 (1968).
3. N. Basco and K. K. Yee, *Spectrosc. Lett.* **1,** 17–18 (1968).
4. T. Ni, Q. Lu, X. Ma, S. Shuqin, and F. Kong, *Chem. Phys. Lett.* **126,** 417–420 (1986).
5. G. S. Jackel and W. Gordy, *Phys. Rev.* **176,** 443–452 (1968).
6. G. W. Hills, W. J. McCoy, and R. E. Muenchausen, *J. Opt. Soc. Am.* **72,** 1778 (1982).
7. K. D. Hensel, R. A. Hughes, and J. M. Brown, *J. Chem. Soc., Faraday Trans.* **91,** 2999–3004 (1995).
8. H. Fujiwara, K. Kaori, O. Hiroyuki, and S. Saito, *J. Chem. Phys.* **109,** 5451–5355 (1998).
9. H. Fujiwara and S. Saito, *J. Mol. Spectrosc.* **192,** 399–405 (1998).
10. L. Alberts and N. C. Handy, *J. Chem. Phys.* **89,** 2107–2115 (1988).
11. K. Balasubramanian, *J. Chem. Phys.* **91,** 2443–2451 (1989).
12. R. C. Binning and L. A. Curtiss, *J. Chem. Phys.* **92,** 1860–1864 (1990).
13. T. J. Sears, P. R. Bunker, A. R. W. MacKellar, K. M. Evenson, D. A. Jennings, and J. M. Brown, *J. Chem. Phys.* **77,** 5348–5362 (1982).
14. I. C. Bowater, J. M. Brown, and A. Carrington, *Proc. Roy. Soc. London, Ser. A* **333,** 265–288 (1973).
15. J. K. G. Watson, "Vibrational Spectra and Structure, Vol 6," (J. R. Durig, Ed.), Elsevier, New York, 1977.
16. J. M. Brown and T. J. Sears, *Mol. Phys.* **75,** 111–113 (1979).
17. T. J. Sears, *Comput. Phys. Rep.* **2,** 1–32 (1984).
18. T. J. Sears, *Comput. Phys. Commun.* **34,** 123–133 (1984).
19. P. B. Davies, D. K. Russell, B. A. Thrush, and H. E. Radford, *Proc. Roy. Soc. London, Ser. A* **353,** 299–318 (1977).
20. T. Hirao, S. Hayakashi, S. Yamomoto, and S. Saito, *J. Mol. Spectrosc.* **187,** 153–162 (1998).
21. L. Hedberg and I. M. Mills, *J. Mol. Spectrosc.* **160,** 117–142 (1993).
22. A. Carrington, "Microwave Spectroscopy of Free Radicals," Academic Press, San Diego, CA, 1974.
23. R. F. Curl, *Mol. Phys.* **9,** 585–597 (1965).
24. K. Dressler and D. A. Ramsay, *Philos. Trans. R. Soc. Lond. A, Math. Phys. Sci.* **251,** 553–581 (1959).
25. R. N. Dixon, *Mol. Phys.* **10,** 1–6 (1965).
26. W. Weltner, "Magnetic atoms and molecules," Van Nostrand Reinhold, New York, NY (1983).
27. J. Kong, L. A. Eriksson, and R. J. Boyd, *Chem. Phys. Lett.* **217,** 24–30 (1994).
28. M. T. Nguyen, S. Creve, L. A. Eriksson, and L. G. Vanquickenborne, *Mol. Phys.* **91,** 537–550 (1997).
29. H. S. P. Müller, H. Klein, S. P. Belov, G. Winnewisser, I. Morino, K. M. T. Yamada, and S. Saito, *J. Mol. Spectrosc.* **195,** 177–184 (1999).
30. M. Kajita, Y. Endo, and E. Hirota, *J. Mol. Spectrosc.* **124,** 66–71 (1987).
31. W. Gordy and R. L. Cook, "Techniques of Chemistry, **18,** Microwave Molecular Spectra," 3rd ed., Wiley-Interscience, New York, 1984.
32. I. M. Mills, T. Cvitaš, K. Homann, N. Kallay, and K. Kuchitsu, "Quantities, Units and Symbols in Physical Chemistry," 2nd ed., Blackwell Scientific, Oxford, 1993.
33. H. Lefebvre-Brion and R. W. Field, "Perturbations in the Spectra of Diatomic Molecules," Academic Press, San Diego, CA, 1986.